European Journal of Mechanics A/Solids 65 (2017) 324–335

Contents lists available at ScienceDirect

European Journal of Mechanics A/Solids

journal homepage: www.elsevier.com/locate/ejmsol

Mesh influence in orthogonal cutting modelling with the Coupled Eulerian-Lagrangian (CEL) method

F. Ducobu*, E. Rivière-Lorphèvre, E. Filippi

University of Mons (UMONS), Faculty of Engineering (FPMs), Machine Design and Production Engineering Lab, 20 Place du Parc, B-7000 Mons, Belgium

ARTICLE INFO

Article history:
Received 18 November 2016
Received in revised form
18 April 2017
Accepted 26 May 2017
Available online 1 June 2017

Keywords:
Benchmark
Coupled Eulerian-Lagrangian (CEL)
Mesh dependence
Orthogonal cutting
Ti6Al4V

ABSTRACT

Metal cutting is nowadays mostly modelled with the Lagrangian formalism when the finite element method is adopted. With these models, the results depend on the mesh parameters, such as the elements size, orientation, etc. While this is a known problem, few studies that analyse it systematically and quantitatively can be found. The Coupled Eulerian Lagrangian (CEL) formalism is an attractive alternative to the Lagrangian formulation. The mesh dependency issue has still to be highlighted when CEL is adopted. The aim of this paper is to study the mesh influence on the results of a CEL model and to provide recommendations for future modelling. A benchmark is carried out based on an experimental reference in strictly orthogonal cutting conditions. The comparison of the numerical results with this reference shows that the size of the elements influences significantly the chip morphology and the cutting forces. This size should be at least two times smaller than the cutting edge radius of the tool to obtain results with an acceptable accuracy. The orientation of the elements is an important parameter as well. It is such that it is recommended to use square elements to avoid any influence of the elements orientation on the results. On the contrary, the results are independent of the elements size and number in the direction perpendicular to the cutting plane. For the cutting conditions of this study, square elements of 5 μm size should be used to obtain converged numerical results.

1. Introduction

The cutting process is complex and involves many phenomena. Numerical modelling contributes to study and master the cutting process, up to now mostly in the particular (and simplified) configuration of orthogonal cutting. Eulerian and Lagrangian models are found in the literature with different variations (Arrazola et al., 2013), each having their pros and cons. The Coupled Eulerian Lagrangian (CEL) formulation has recently been successfully applied to numerical modelling of orthogonal cutting and overcomes many disadvantages of the other methods (Ducobu et al., 2016a). It turned out to be an attractive alternative to them.

A major concern when developing a finite element model is the mesh dependence of the results. The problem of mesh dependence has to be solved early in the development of the model because it will influence the results. Then, the model is ready to be improved with the optimal mesh that is not a parameter any more. This issue of mesh dependence has therefore to be handled as well when modelling the process of orthogonal cutting. The CEL method has not been widely used for cutting modelling so far and no study on the mesh dependency of the results for this application is available. This mesh issue has only briefly been addressed for geomechanical problems with large deformations (Qiu et al., 2011). Four elements sizes were considered for square elements and convergence was reached when the elements size is small enough. This shows that the mesh dependence in CEL models is an issue as well and it should therefore be addressed for orthogonal cutting. To be consistent with the current literature for orthogonal cutting modelling with (most widespread) Lagrangian models, this work will rely on the information that can be found for that formalism.

Bäker et al. (2003) compared the results of two different mesh densities for a 2D model with remeshing and without taking damage into account. The Ti6Al4V chips formed were segmented (or saw-toothed) and geometrically rather close. The finer mesh however provided more details in the shear band. A difference in the cutting force of around 5% was observed; the finer mesh lead to a lower value. For a 2D model of Ti6Al4V orthogonal cutting with damage and a segmented chip produced, Zhang et al. (2011b) compared the average cutting force values of four elements sizes

* Corresponding author..
E-mail address: Francois.Ducobu@umons.ac.be (F. Ducobu).

http://dx.doi.org/10.1016/j.euromechsol.2017.05.007
0997-7538/

to an experimental value. A mesh dependence was noted. The two large sizes lead to an average value smaller than the reference and a difference between both numerical results occurred. On the contrary, the two small elements sizes gave both a value close to the experimental reference.

Barge et al. (2006) showed for a 2D orthogonal cutting model of AISI 4142 with damage that the elements size (four values were considered for square elements) has a marginal influence on the cutting force but that higher variations were observed for a larger mesh. The chip morphology was more affected. Continuous chips were formed and the main difference concerned their curvature. The authors highlighted the importance of the experimental reference in order to validate a numerical model due to the mesh dependency of the results. According to Ambati and Yuan (2011), the chip morphology should be used to characterize the quality of the numerical results and the main parameter to validate a model is the cutting force value. For a 2D model of AISI 4340 cutting with damage, they highlighted a significant influence of the elements size on the chip morphology for two different mesh densities. The chip type could even change from continuous to segmented for a finer mesh. The average value of the cutting force for three different elements sizes was nearly the same. Higher forces variations were observed for a coarser mesh due to the higher discontinuity introduced by the suppression of a larger element. Dependence of chip morphology and cutting force average value to the mesh size were observed as well for the finite element model of Shams and Mashayekhi (2012) for A2024-T351.

A more detailed study of the mesh influence (elements size, elements orientation, elements interpolation order) on the results has been carried out by Hortig and Svendsen (2007) when modelling segmented Inconel 718 chip with damage. In addition to the study of the elements size dependency over the results, they also showed that their orientation strongly influenced the chip morphology and the cutting force. An increase of the chip segmentation frequency was observed when the elements size was smaller, as well as a reduction of the cutting force average value.

The literature review shows that, although of significant importance, the mesh dependency in finite element modelling has not been studied that much and no clear guidelines can be found in the literature when developing a model. The literature review has shown, for example, the sensitivity of the cutting force to the mesh density. Depending on the source, the evolution is however not the same: it can decrease with the elements size (Bäker et al., 2003; Hortig and Svendsen, 2007), increase for smaller elements (Zhang et al., 2011b) or even not be significantly affected (Ambati and Yuan, 2011; Barge et al., 2006). Mesh influence is as well not clearly defined as it usually concerns the elements size (Ambati and Yuan, 2011; Bäker et al., 2003; Barge et al., 2006; Shams and Mashayekhi, 2012; Zhang et al., 2011b) but elements orientation and interpolation order as well (Hortig and Svendsen, 2007). The validation of the converged mesh parameters is moreover not based systematically on the same experimental parameters, nor for a given set of cutting conditions. Average cutting force value and qualitative chip morphology are the most used points of comparison. A lack of benchmark with detailed, systematic and quantitative comparisons is brought out of the literature when the modelling of orthogonal cutting is considered with Lagrangian models.

This paper studies the influence of the mesh on the results of an orthogonal cutting CEL model of Ti6Al4V. Three mesh parameters are selected: the size of the elements, the orientation of the elements and the size (and the number) of elements in the width of the model (i.e. in the direction normal to the cutting plane). The interpolation order and the element type (number of nodes per element, for example) are not included because only one element type is currently available in Abaqus/Explicit v6.14-2 (H.K.S., 2014) for a CEL model. The comparison data with the experimental reference are the chip morphology (shape and characteristic length), the temperature fields and the cutting forces (temporal evolution and RMS value). The complete study (with the three mesh parameters) is carried out for an uncut chip thickness of 40 μm. Two other uncut chip thicknesses values (60 μm and 100 μm) are adopted in a second time, while the elements size is the only parameter considered. The importance of the experimental reference has been highlighted in the literature review. The specific configuration of the tests provides a direct point of comparison with the modelling as it allows to provide strictly orthogonal cutting experimental results. The experiments are briefly described as well. Their results constitute a reference on which this, but future also, numerical studies can rely on. Following the confrontation with the experimental reference, some recommendations are provided for future modelling of orthogonal cutting.

2. Experimental reference

The experimental reference is provided by experiments carried out in strictly orthogonal cutting conditions. This allows to compare directly the experimental results to modelling results. Fig. 1 shows the particular configuration of the experiments, introduced by the authors in Ducobu et al. (2015b), on a five-axis high speed milling machine used as a planning machine. Table 1 presents the cutting conditions adopted in the experiments and the tool geometry. The tool was custom made by SECO from a standard LCGN160602-0600-FG-X tool. The machined material was the Ti6Al4V titanium alloy. Three uncut chip thicknesses, h, were chosen: 40 μm, 60 μm and 100 μm at a single cutting speed, 30 m/min, the highest feed rate of the machine. Each test was repeated minimum three times. The cutting forces were measured with a Kistler 9257B dynamometer. The chips were collected and then observed with an optical microscope after being etched by Kroll's reagent to reveal the Ti6Al4V microstructure (β phase coloured in dark brown, i.e.

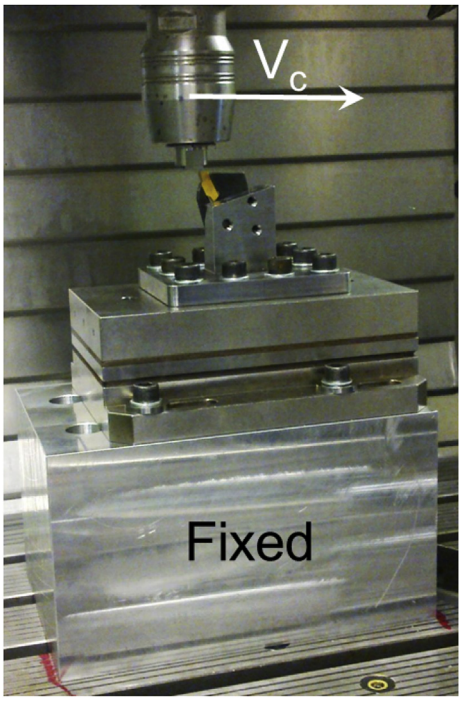

Fig. 1. Orthogonal cutting configuration: workpiece in the spindle (moving at the cutting speed, V_c) and tool fixed on the machine table (Ducobu et al., 2015b).

Table 1
Cutting conditions of the experiments (Ducobu et al., 2015b).

Cutting speed (m/min)	30
Uncut chip thickness (μm)	40, 60, 100
Width of cut (mm)	1
Length of cut (mm)	10
Rake angle (°)	15
Clearance angle (°)	2
Cutting edge radius (μm)	20

Table 2
Chip thickness, h', for 25 measurements and cutting forces at the three uncut chip thicknesses (Ducobu et al., 2015b).

	40 μm	60 μm	100 μm
h' (μm)	59 ± 5	80 ± 4	135 ± 6
RMS CF (N/mm)	86 ± 2	113 ± 2	174 ± 2
RMS FF (N/mm)	40 ± 1	44 ± 1	50 ± 1

black on the microscope views).

Sections of the chips at the three uncut chip thicknesses are provided in Fig. 2(a) to (c). All of them were continuous chips. Continuous chips were requested in this study to allow the comparison between the different meshes without influence of particular phenomena, such as strain softening or damage, occurring during the formation of chips that are not continuous such as segmented chips.

The short cutting length (10 mm) provided chips that did not need to be unrolled and therefore deformed before embedding. This will allow to directly compare experimental and numerical chip thickness, h', values. Table 2 presents the mean values of the three chip thicknesses; 25 measurements were taken along each chip to compute the mean. The standard deviation values are also provided in the table; they are lower than 10% of the chip thickness.

The cutting and feed forces were nearly constant on the whole cutting length due to the continuous chip morphology. The average values of the root mean square (RMS) forces are given in Table 2 for the three uncut chip thicknesses. As expected, the forces are increasing with the uncut chip thickness. It is noted that the standard deviation values are low for the three uncut chip thicknesses.

3. CEL finite element model

The application of the CEL method to model the metal cutting has been introduced in Ducobu et al. (2016a). In this model, the tool is described by a Lagrangian formulation while the workpiece is described by an Eulerian formulation. The Eulerian area includes the initial shape of the workpiece and the area where the chip will form, i.e. where the machined material can be found during the computation. This implies that the initial void above the workpiece is also meshed, which increases the number of elements by comparison to a Lagrangian model. The study carried out in this paper will be based on a finite element model with similar characteristics as in Ducobu et al. (2016a). Only 3D 8-node brick elements are available in Abaqus/Explicit v6.14-2 (H.K.S., 2014) for the CEL formalism. To limit the number of degrees of freedom, there is a single element out of the cutting plane; its width is 50 μm. Fig. 3 presents schematically the initial geometry of the models and the

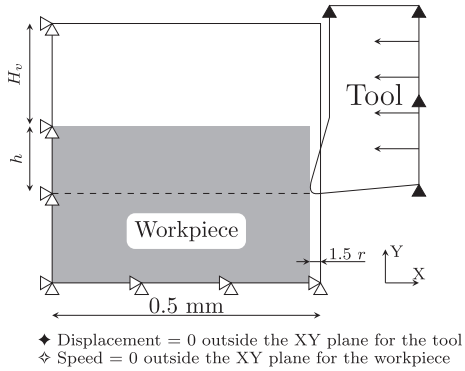

Fig. 3. Schematic initial geometry and boundary conditions of the models (r: cutting edge radius, h: uncut chip thickness, H_v: height of the area initially filled with void).

boundary conditions. The dimensions of the workpiece are defined depending on the cutting edge radius of the tool, r, and the uncut chip thickness, h. The length of the workpiece is set to 0.5 mm to allow a cutting time of 600 μs, which is sufficient to reach the steady-state of the cutting forces and a chip long enough to be measured. The height of the area filled with void at the beginning of the cut, H_v, depends on the value of h and is chosen to prevent the Eulerian material to flow out of the domain. An example of initial mesh is shown in Fig. 4. To have a model as close as possible to a 2D plain strain one, the displacements out of the cutting plane of the Lagrangian nodes (tool) have been constrained, while the speed out of the plane of the Eulerian nodes (workpiece) has been constrained. The moving part is the tool like in classic transient Lagrangian models. Its geometry is the same as in the experiments (Table 3). The tool is meshed with 3D 8-node brick elements (4 nodes in the cutting plane). It is composed of 75 elements and 188 nodes. In the cutting plane, the length of the elements composing the edge radius is 4.66 μm to allow modelling the radius of 20 μm. The elements size grows then when moving away of the radius.

The Johnson-Cook (JC) constitutive model (Johnson and Cook, 1983) is the most popular model used in cutting process simulation. It does not take strain softening into account contrary to more

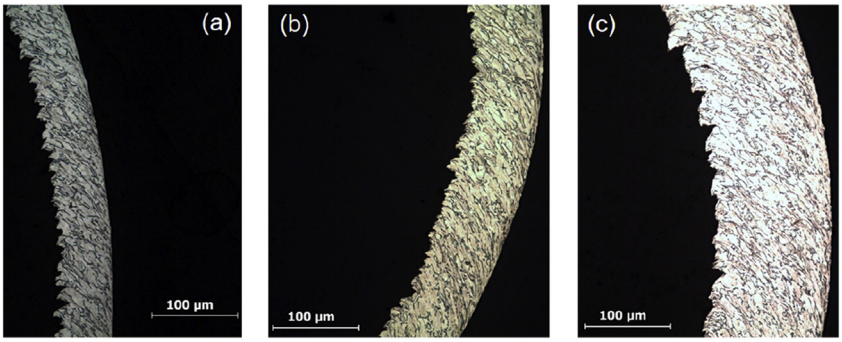

Fig. 2. Optical microscope chips sections (a) 40 μm, (b) 60 μm and (c) 100 μm (Ducobu et al., 2015b).

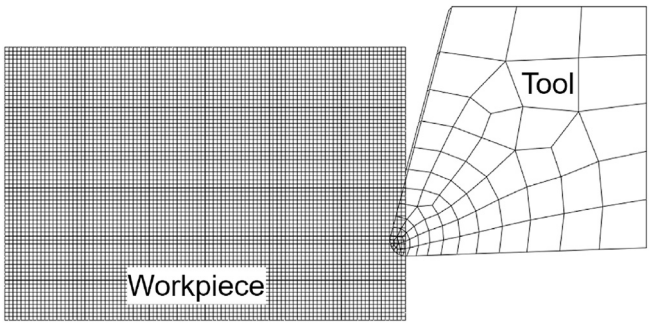

Fig. 4. Initial mesh for 5 μm length square elements and $h = 40$ μm.

recent models (Ducobu et al., 2015a). It is however well suited to describe the behaviour of Ti6Al4V in this study as continuous chips were experimentally formed. It will therefore make no difference in the results whether the strain softening is taken into account or not. The JC model is composed of three independent terms dissociating plastic, viscous and thermal aspects:

$$\sigma = (A + B\varepsilon^n)\left(1 + C\ln\frac{\dot{\varepsilon}}{\dot{\varepsilon}_0}\right)\left(1 - \left[\frac{T - T_{room}}{T_{melt} - T_{room}}\right]^m\right) \quad (1)$$

In this equation, A, B, C, m and n are material properties. The melting temperature is T_{melt}, the room temperature is T_{room} and the reference strain rate is $\dot{\varepsilon}_0$. The selected set of parameters of this study is given in Table 3.

Tungsten carbide (tool material) is described by a linear elastic model. The materials properties of both materials are given in Table 3. Friction at the tool – chip interface is modelled with a Coulomb coefficient value of 0.2, according to the experimental study of Rech et al. (2013) for the same tool – workpiece couple and the same cutting speed, in dry cutting conditions. Equal repartition of the heat generated by friction (efficiency of friction to heat conversion is assumed to be 100%) between the tool and the chip is adopted, in accordance with values provided by Rech et al. (2013). They used a special tribometer reproducing the sliding velocities and contact pressures occurring during machining. They applied then an analytical procedure to identify the values of the friction coefficient and of the heat partition. They provided both global and local friction coefficients. The local coefficient value is selected for the model of this study, as intended by Rech et al. (2013) in their paper. All the faces are adiabatic and the efficiency of deformation to heat conversion is 90% (Nasr et al., 2007).

Table 3
Material properties and cutting conditions of the numerical model (Lampman, 1990; Meyer and Kleponis, 2001; Nasr et al., 2007; Özel and Zeren, 2007; Rech et al., 2013; Sun and Guo, 2009).

JC constitutive model	A (MPa)	862
	B (MPa)	331
	C	0.012
	m	0.8
	n	0.34
	$\dot{\varepsilon}_0$	1
	T_{room} (K)	298
	T_{melt} (K)	1878
Inelastic heat fraction	Ti6Al4V	0.9
Density, ρ (kg/m^3)	Ti6Al4V	4430
	Carbide	15,000
Young's modulus, E (GPa)	Ti6Al4V	113.8
	Carbide	800
Poisson's ratio, ν (–)	Ti6Al4V	0.342
	Carbide	0.2
Expansion, α (K^{-1})	Ti6Al4V	8.6 e^{-6}
	Carbide	4.7 e^{-6}
Conductivity, k (W/mK)	Ti6Al4V	7.3
	Carbide	46
Specific heat, c_p (J/KgK)	Ti6Al4V	580
	Carbide	203
Friction coefficient		0.2
Friction energy to heat (%)		100
Heat partition to part (%)		50
Cutting speed, V_c (m/min)		30
Uncut chip thickness, h (μm)	40, 60, 100	
Rake angle, γ (°)		15
Clearance angle, α (°)		2
Cutting edge radius, r (μm)		20

4. Mesh size influence

The length of the elements in the cutting plane is the first parameter to be studied. The uncut chip thickness is fixed at 40 μm. To avoid any preferred direction, the shape of the elements is a square. Their edge length will vary to highlight its influence on the results. The tool edge radius value is chosen to define the largest element length, 20 μm. The other elements lengths adopted, 10 μm, 5 μm and 2.5 μm, are given in Table 4 with the number of elements and nodes of the workpiece ($H_v = 220$ μm).

The four corresponding chips are presented in Fig. 5. As in the experiments (Fig. 2), they are all continuous. At 5 μm and 2.5 μm, the shape of the chip is more detailed than for the two larger ones. At 20 μm, the chip is highly rounded and its shape is rather rough. At 10 μm, the chip is still rounded but less. The chip curvature radius, and therefore the rigidity of the chip, decrease with the elements size; a stabilization is observed from 5 μm. A significant and unrealistic gap appears between the clearance face and the machined surface at 20 μm. This gap is nearly unnoticeable at 10 μm and it disappears for smaller elements.

Table 5 presents the chip thickness values of the four models. All of them are larger than the experimental reference. It is 17% larger at 20 μm and 10% larger with the other elements lengths. So, at 10 μm, the shape of the chip is more rounded due to the larger elements but the chip thickness is correctly modelled. Again, an element length of 20 μm leads to results of lower quality. As mentioned in Ducobu et al. (2016a), a higher numerical value of the chip thickness could be expected. In the experiments, the chip can expand laterally, while it is not allowed in the modelling and may contribute to the larger numerical chip thickness.

Temperature fields are plotted in Fig. 5. They are similar for the four elements sizes. The high temperature area is however larger at 20 μm, as well as the maximum temperature value. For all the models, the highest temperature is found in the workpiece in the area near the tool edge radius and in the secondary shear zone. The highest temperature was expected in the secondary shear zone. The high temperatures location is therefore correctly estimated.

The numerical forces evolutions versus time are plotted in Fig. 6 together with the experimental RMS values. Steady-state of the numerical forces is reached after less than 150 μs. Numerical RMS values of the forces are provided in Table 5. The forces at 20 μm are significantly different than the other ones. A cyclic evolution of both cutting (in the X direction) and feed (in the Y direction) forces is noted, as well as larger RMS values. This forces evolution is not

Table 4
Number of elements and nodes for the four square elements lengths.

Length (μm)	Elements	Nodes
20	425	936
10	1700	3570
5	6800	13,938
2.5	27,200	55,074

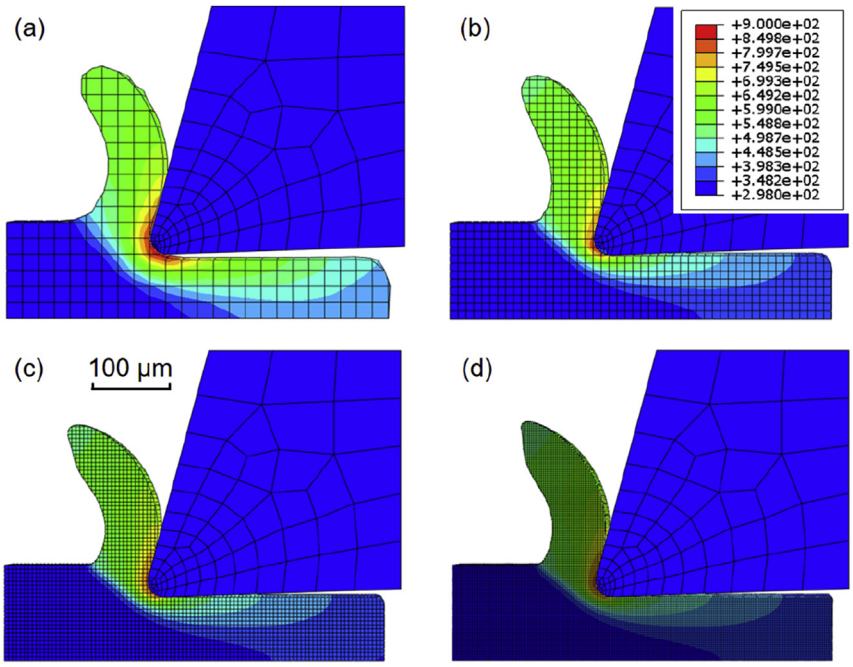

Fig. 5. Temperature contours (in K) of the numerical chips with square elements (a) 20 µm, (b) 10 µm, (c) 5 µm and (d) 2.5 µm after 600 µs of cutting.

Table 5
RMS cutting forces and chip thickness summary for square elements, Δ_x: difference with the experimental values.

Case	CF (N/mm)	Δ_{CF} (%)	FF (N/mm)	Δ_{FF} (%)	h' (µm)	$\Delta_{h'}$ (%)
Exp.	86 ± 2	–	40 ± 1	–	59 ± 5	–
20	78	9	37	8	69 ± 2	−17
10	67	22	29	28	65 ± 1	−10
5	66	23	31	23	65 ± 1	−10
2.5	65	24	33	18	65 ± 1	−10

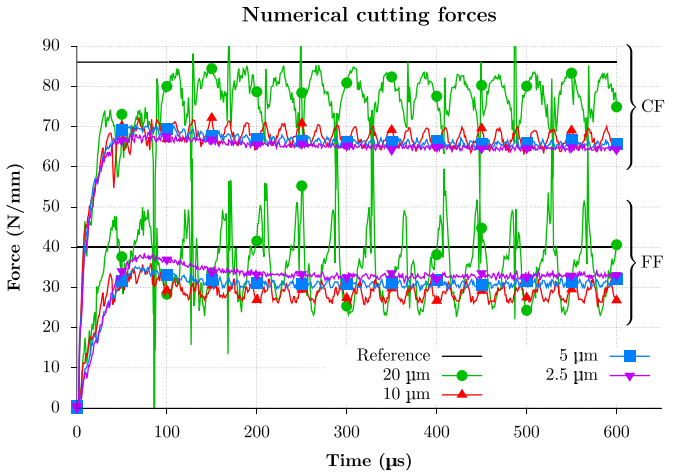

Fig. 6. Numerical cutting forces with square elements.

linked to the formation of a continuous chip that should lead to a nearly constant value of the forces. The number of cycles is actually related to the number of elements crossed by the tool. High transient values are observed as well for this elements size.

This phenomenon of forces variations linked to the elements is also observed at 10 µm. Their frequency is two times larger, like the number of elements. The magnitude of their variation is lower but still noticed. This time, the RMS values are however not affected as they are close to values at 5 µm and 2.5 µm. For the two smallest elements lengths, the variation of the forces around the mean value is not significant (it is a classic noise) and the RMS values are nearly equal (Table 5). These evolutions are typical of a continuous chip. By comparison with the experimental RMS values, the numerical forces are lower of less than 25% for both cutting and feed forces. The forces at 20 µm are closer to the reference (less than 10% lower) but their evolutions are too far from a nearly constant value. Lower numerical forces values with this set of JC parameters have previously been mentioned in the literature (Ducobu et al., 2016b; Umbrello, 2008). The values and differences presented in Table 5 are therefore in accordance with the previous works from the current state of the art. The main objective of this paper is to study the influence of the mesh on the results. Such a difference in the forces value has therefore no influence on the observations and conclusions that will be drawn.

Computation time is not provided in the article due to limitations linked to calculations running on a supercomputer. Indeed, it makes no sense to compare the computation times because, for the same simulation, they vary greatly (of more than ± 20%) depending on the load of the supercomputer. This load cannot, of course, be controlled by the authors and it is then not possible to obtain reliable and reproducible computing times. Anyway, to give an order of magnitude of computing times, around 285 min are needed to compute 600 µs of simulation for the model with 5 µm square elements with 4 Intel SandyBridge 2.60 GHz processors.

When decreasing the length of square finite elements from 20 µm to 2.5 µm, an evolution in the results (chip morphology, temperatures and forces) is noted. A significant difference is observed between 20 µm and 10 µm. The transition from 10 µm to 5 µm highlights fewer differences and nearly none is noted between 5 µm and 2.5 µm. This shows that convergence is reached. To limit the computing resources, it is recommended to consider the 5 µm element length for future modelling.

5. Mesh orientation influence

The orientation of the mesh is the second parameter to be studied. The uncut chip thickness is still 40 μm. Two orientations of the elements are considered: parallel and perpendicular to the cutting speed direction. To achieve this, the elements have now a rectangular shape with their length parallel or perpendicular to the cutting speed direction. Two configurations are studied: either the whole workpiece is composed of rectangular elements, either it is composed of a combination of square and rectangular elements.

5.1. Rectangular elements

When only rectangular elements compose the workpiece, the designation of the model is *element length* × *element height* (direction X × direction Y in Fig. 3). Four elements configurations are adopted. The corresponding numbers of elements and nodes of the workpiece are given in Table 6 and the resulting chips in Fig. 7.

All the chips in Fig. 7 are still continuous. Strong differences in the chips morphologies are however noticed. The rigidity is highly influenced by the orientation of the elements. When they are horizontal (Fig. 7(a) and (c)), the rigidity of the chip is higher than when they are vertical (Fig. 7(b) and (d)). The chip thickness is higher as well and the length is shorter. For the 10×20 μm^2 elements (Fig. 7(b)), the very low rigidity and the length lead to a small curvature radius. As for square elements, the value of the elements length influences the roundness and the level of details of the chip shape. Similarly, a gap with the machined surface is observed under the clearance face near the tool edge radius when the size is 20 μm. The four temperature fields are rather close. When the elements are larger, the high temperature area is slightly larger on the rake face, at the beginning of the secondary shear zone. This is due to the longer contact length of the chip on the tool.

As expected from Fig. 7, the chip ticknesses values in Table 7 are larger for horizontal elements. For 10×20 μm^2 elements, the chip thickness is the lowest. The vertical orientation with 5×10 μm^2 elements leads to a chip thickness very close to the experimental value. This value is slightly lower than that for 5 μm square elements. Vertical rectangular elements tend to increase the chip length and decrease the chip thickness. A lower value of the chip thickness could therefore be expected. The orientation of the elements has a strong influence on the chip morphology. The size of the elements has more influence on the chip thickness value when they are oriented vertically.

The same observations are performed on the forces evolutions of Fig. 8 as for square elements. The steady-state is reached before 150 μs and cyclic evolutions with no link with the chip formed are produced when the size of the elements is large. The magnitude of the oscillations around the mean value is larger when the elements orientation is horizontal and the feed force variations are larger than that of the cutting force as it is clearly seen in Fig. 8 for 20×10 μm^2 and 10×20 μm^2. For vertically oriented elements, variations are noted as well but of lower magnitude and this magnitude is larger in the horizontal direction. The frequency of the variations of

Table 6
Number of elements and nodes for the rectangular elements.

Model (μm^2)	Elements	Nodes
20×10	850	1820
10×20	850	1836
10×5	3400	7038
5×10	3400	7070

Table 7
RMS cutting forces and chip thickness summary for rectangular elements, Δ_x: difference with the experimental values.

Case	CF (N/mm)	Δ_{CF} (%)	FF (N/mm)	Δ_{FF} (%)	h' (μm)	$\Delta_{h'}$ (%)
Exp.	86 ± 2	–	40 ± 1	–	59 ± 5	–
20×10	74	14	39	3	72 ± 0	−22
10×20	63	27	27	33	45 ± 1	24
10×5	67	22	31	23	70 ± 1	−19
5×10	67	22	33	18	61 ± 1	−3

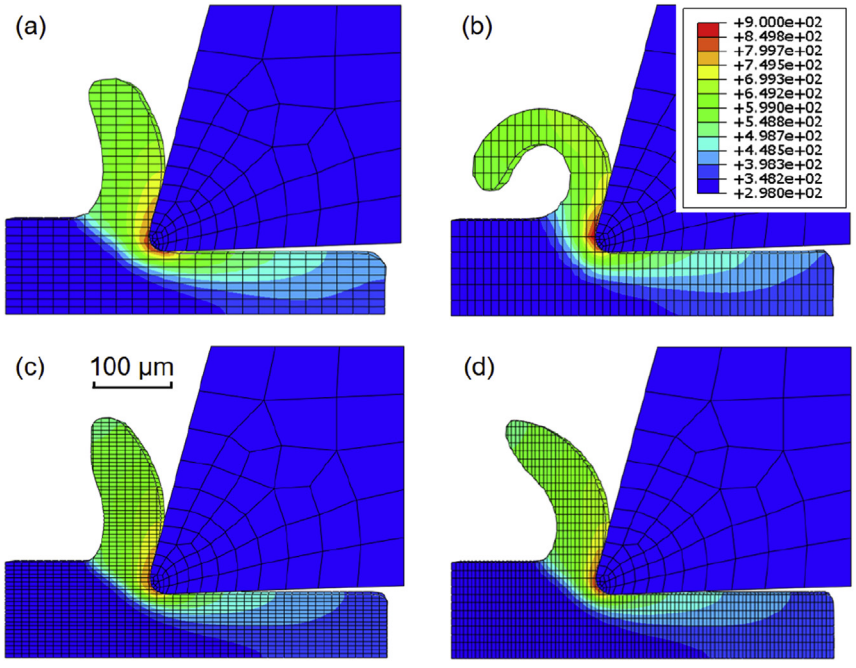

Fig. 7. Temperature contours (in K) of the numerical chips with rectangular elements (a) 20×10 μm^2, (b) 10×20 μm^2, (c) 10×5 μm^2 and (d) 5×10 μm^2 after 600 μs of cutting.

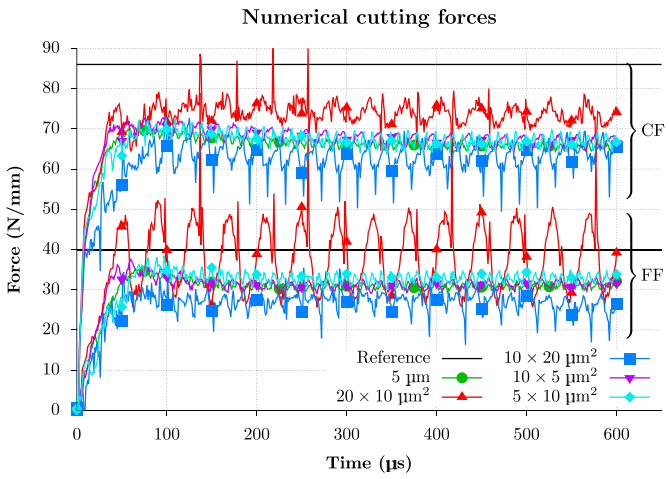

Fig. 8. Numerical cutting forces with rectangular elements.

these two models is different by a ratio of two: it is two times larger for vertical than for horizontal ones.

The RMS values of the cutting forces are therefore larger for 20 × 10 µm^2 than the three other models (Table 7). The chip at 10 × 20 µm^2 has a low rigidity; lower RMS values of the forces could be expected. The RMS values of the two other models are very close, as are their forces evolutions. Differences in the chip morphologies are however noted. By comparison to the experimental reference, the forces values of these models are similar to these with square elements.

The orientation of the elements has a high influence on the chip morphology and the forces evolutions. Horizontally oriented elements lead to a shorter and wider chip than vertically oriented elements for which the chip is longer, thinner and less rigid. Concerning the cutting forces, significant variations are obtained with large elements but they are higher for horizontal elements. The frequency of the variations depends on the number of elements in the cutting direction and the magnitude of the variations is larger in the direction corresponding to the shorter side of the rectangular elements.

Table 8
Number of elements and nodes for the models with square and rectangular elements.

Model	Elements	Nodes
Comb1	2900	6060
Comb2	1050	2244
Comb3	525	1144

5.2. Square and rectangular elements

Three meshes combining square and rectangular elements are adopted. The workpiece of *Comb1* model is composed of 5 × 20 elements, excepted in the upper part of the area initially filled with Ti6Al4V (dark grey zone in Fig. 3) where 5 µm square elements are used. The workpiece of *Comb2* is composed of 10 × 20 elements and 10 µm square elements and in *Comb3*, of 20 µm square elements and 20 × 10. The objectives of the combination are to reduce the number of degrees of freedom of the model (Table 8) by comparison with models made of only square elements, while keeping a good quality of the results. In *Comb1* and *Comb2*, square elements are defined where the chip separates of the workpiece and therefore where the mesh may have more influence on the results. In *Comb3*, rectangular elements allow to have two times more elements in the zone where the chip forms to better capture the phenomena.

Three different chips are produced by the three models (Fig. 9), although they are still continuous. In accordance with previous results, the chip rigidity increases with the length of the elements in the horizontal direction. The chips thicknesses follow the same trend (Table 9). The mean value of *Comb2* is equal to the experimental reference, while *Comb1* is smaller and *Comb3* is larger. The elements are larger in *Comb3* and the gap under the clearance face is high. Temperature fields are similar for *Comb2* and *Comb3* but the high temperatures area is slightly larger for *Comb3*, mainly because of the larger contact length. The temperature in the secondary shear zone for *Comb1* is higher than in the two other models and its area is larger as well. High temperature is even observed outside the tool – chip contact zone and it does not seem realistic. This may be due to the high elongated elements vertically oriented: the ratio of their height on their length is 4, which is larger than the maximum of 2 recommended as a good practice rule in Lagrangian finite elements (Ducobu et al., 2015c). High ratio elements should therefore be avoided in CEL modelling as well.

The forces evolutions (Fig. 10) of *Comb3* confirm that horizontal elements lead to high forces variations and that they are higher in the direction of the elements width. The elements topology is the same for *Comb1* and *Comb2*, the difference is the larger elements size for *Comb2*. The larger elements of *Comb2* lead to larger forces variations. The magnitude of the variations seems close in both directions, indicating that they are caused by elements in the chip separation area. This is in accordance with the forces evolutions of *Comb3*. The RMS values follow the previously highlighted trends (Table 9). The only significant difference is the feed on cutting forces ratio that is 0.6 for *Comb3*, while it is often slightly under 0.5 for all the previous models.

Combining square and rectangular elements allows to reduce the number of elements by comparison to square elements. The disadvantages of large square elements and rectangular elements, even when they are not in the chip separation area, are still observed and influence the results. Rectangular elements with high

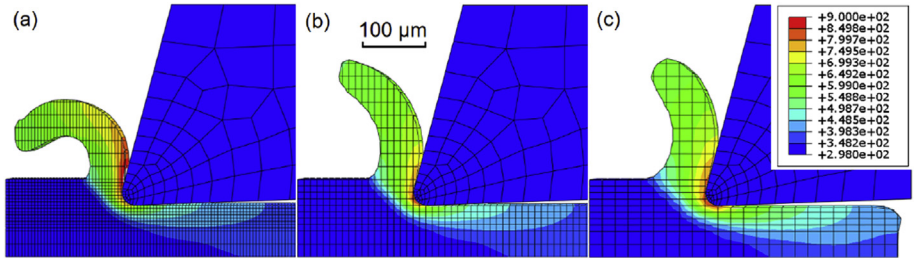

Fig. 9. Temperature contours (in K) of the numerical chips with square and rectangular elements (a) *Comb1*, (b) *Comb2* and (c) *Comb3* after 600 µs of cutting.

Table 9
RMS cutting forces and chip thickness summary for the models with square and rectangular elements, Δ_x: difference with the experimental values.

Case	CF (N/mm)	Δ_{CF} (%)	FF (N/mm)	Δ_{FF} (%)	h' (μm)	$\Delta_{h'}$ (%)
Exp.	86 ± 2	–	40 ± 1	–	59 ± 5	–
Comb1	59	31	32	20	55 ± 1	7
Comb2	63	27	30	25	59 ± 2	0
Comb3	70	19	42	−5	65 ± 2	−10

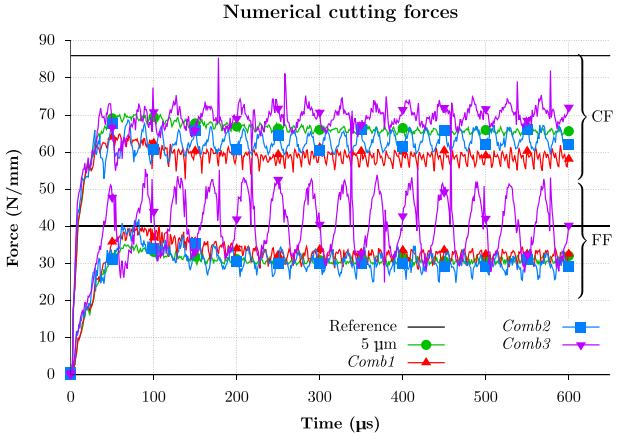

Fig. 10. Numerical cutting forces with square and rectangular elements.

height on length ratio produce unrealistic results and should be avoided.

6. Time increment

Cyclic evolutions of the forces are observed for large elements regardless of their shape and orientation. The explicit formulation is adopted in this study and the length of the elements of the mesh directly influences the stable time increment. This paragraph is intended to look at the influence of the time increment on the cyclic evolutions of the forces.

The stable time increment, Δt_{stable}, is calculated from the properties of mass and stiffness of the entire system. Without damping it is given by (Bathe and Wilson, 1976; Cocchetti et al., 2012; Koric et al., 2009)

$$\Delta t_{stable} = \frac{T_{min}}{\pi} = \frac{2}{\omega_{max}} \tag{2}$$

where T_{min} is the smallest eigenvalue of the finite element model and ω_{max} is its largest eigenfrequency.

To avoid having to calculate the eigenvalues, the stability limit is calculated in practice by (Koric et al., 2009)

$$\Delta t_{stable} = min\left(\frac{L_c}{C_d}\right) \tag{3}$$

with L_c the characteristic length of each element of the mesh and C_d the wave propagation speed in the material. In Abaqus, the characteristic length of an element, L_c, is defined as the square root of its surface (H.K.S., 2014). The wave propagation speed in the material, C_d, is computed by

$$C_d = \sqrt{\frac{\lambda + 2\mu}{\rho}} \tag{4}$$

where ρ is the density and λ and μ are Lamé's coefficients. For an elastic isotropic material, the two coefficients are given by

$$\lambda = \frac{E \cdot \nu}{(1+\nu)\cdot(1-2\nu)} \tag{5}$$

$$\mu = \frac{E \cdot \nu}{2\cdot(1+\nu)} \tag{6}$$

with E Young's modulus of the material and ν Poisson's coefficient.

Table 10 gives stable time increment values, Δt_{stable}, for square elements of 2.5 μm, 5 μm, 10 μm and 20 μm. The time increment values adopted by Abaqus after 600 μs of computation, Δt_{Abq}, are given in Table 10 as well. The time increment values adopted by Abaqus are smaller than the stable time increment values for the 4 meshes. The time increment increase with the elements length therefore does not influence the forces evolutions.

It must be noted that the time increment in Abaqus is equal for meshes of 5 μm, 10 μm and 20 μm. This is because the smallest elements are not in the workpiece for these meshes lengths but in the tool. Indeed, elements in the tool edge radius area must be small enough to allow the modelling of the radius of 20 μm. Their length is 4.66 μm, corresponding to a stable time increment of 8.92 e^{-10} s; the value adopted by Abaqus is larger: 3.18 e^{-10} s. So, the increase of the element length in the workpiece above 4.66 μm does not impact the time increment adopted in Abaqus.

Moreover, the modelling results show that the orientation of the elements (horizontal or vertical) when they are not a square influences the forces evolutions for the same element dimensions. The stable time increment is computed with the characteristic length of the elements. This characteristic length is the same for a horizontal and a vertical element. So, the stable time increment is not modified by the orientation of the elements composing the mesh.

Finally, the frequency of the cutting force evolutions, f_{CF}, is compared to the frequency of the time increment, $f_{\Delta t}$. For elements of 2.5 μm, the cutting force evolutions cannot be determined due to the frequency output of the results which is too low to have enough points to describe the evolution (and the amplitude of this evolution is very small). However, it was observed that the frequency of the forces evolutions is linked to the number of elements crossed by the tool. This frequency can therefore be computed by

$$f_{CF} = \frac{V_c}{L} = 200 \text{ kHz} \tag{7}$$

for an element length, L, of 2.5 μm. For the 3 other elements sizes, the frequencies are given in Table 10 by estimation from the cutting

Table 10
Stable time increment, Δt_{stable}, Abaqus time increment after 600 μs of computing, Δt_{Abq}, frequency of the time increment, $f_{\Delta t}$, and frequency of the cutting force evolution, f_{CF}, for square elements with a length of 2.5 μm, 5 μm, 10 μm and 20 μm (∗: computed value).

Length (μm)	Δt_{stable} (s)	Δt_{Abq} (s)	$f_{\Delta t}$ (Hz)	f_{CF} (Hz)
2.5	4.79 e^{-10}	2.49 e^{-10}	4.02 e^{9}	200 e^{-10} *
5	9.58 e^{-10}	3.18 e^{-10}	3.14 e^{9}	100 e^{3}
10	1.92 e^{-9}	3.18 e^{-10}	3.14 e^{9}	50 e^{3}
20	3.83 e^{-9}	3.18 e^{-10}	3.14 e^{9}	25 e^{3}

evolution. These values are in accordance with Equation (7). The orders of magnitude of the frequency of the cutting force evolutions and of the frequency of the time increment are very different and that the time increment does not influence the frequency of the cutting force evolutions. In the end, it is clear that the time increment does not influence the cyclic evolutions of the forces.

7. Mesh width influence

Up to this point, the influence of the elements size and orientation in CEL cutting modelling has been considered. In this paragraph, the element width, i.e. the length in the direction perpendicular to the cutting plane, will be studied. The elements width adopted so far is 50 μm as in the model introduced in Ducobu et al. (2016a). The size and the orientation of the mesh used are 5 μm square elements. This mesh proved to be the one providing results close to the experiments while preventing any influence of the mesh orientation on the chip morphology and the evolution of the forces.

As already reminded in the paragraph on the mesh orientation influence, a good practice rule in Lagrangian finite elements is to avoid ratios of elements lengths larger than 2. With square elements of 5 μm and 50 μm width, the ratio between the width and the length in the cutting plane is 10. The importance of the value of this ratio for the width will be studied with two models: one with 1 element of 5 μm width (×1) and one with 4 elements in the width (×4) of 50 μm (so the elements width is 12.5 μm). The numerical reference is the model with 5 μm square elements and 1 element in the width of 50 μm (5). Their numbers of elements and nodes are given in Table 11.

Table 11
Number of elements and nodes for the models with width influence.

Model	Elements	Nodes
5	6800	13,938
×1	6800	13,938
×4	27,200	34,845

Fig. 11 presents the results of the two models and the numerical reference chip with 5 μm square elements. The three chips are qualitatively identical. This is confirmed by the value of their chip thickness (Table 12). The width of the elements and their number in this direction do not influence the chip morphology. Temperature fields (Fig. 11) are identical as well. The same results are observed for the cutting forces. The temporal evolutions of the three models are identical (Fig. 12), as well as their RMS values.

The mesh width has therefore no influence on the results. From a computing point of view, it is more efficient to only have 1 element in the width of the model but this width does not alter the quality of the results. The elements width used so far (50 μm) will be kept for future modelling.

8. Mesh size influence at other uncut chip thicknesses

The results of the mesh influence study showed that square elements should be preferred to rectangular ones to avoid influencing mostly the chip morphology. A sensitivity of the elements length, even for a square shape has been shown. The four elements lengths adopted previously will be used to highlight their influence on the results at the two other uncut chip thicknesses of the experiments, 60 μm and 100 μm. Except for the uncut chip thickness value, no changes were implemented in the model in order to obtain a predictive model able to provide quantitative information

Table 12
RMS cutting forces and chip thickness summary for the models with width influence, Δ_x: difference with the experimental values.

Case	CF (N/mm)	Δ_{CF} (%)	FF (N/mm)	Δ_{FF} (%)	h' (μm)	$\Delta_{h'}$ (%)
Exp.	86 ± 2	–	40 ± 1	–	59 ± 5	–
5	66	23	31	23	65 ± 1	−10
×1	67	22	32	20	66 ± 1	- 12
×4	66	23	31	23	66 ± 1	−12

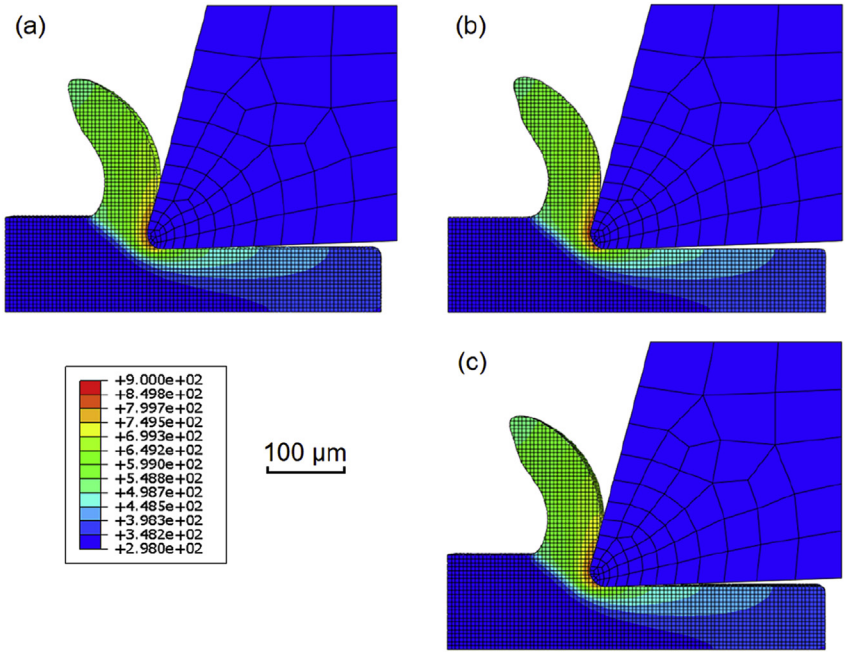

Fig. 11. Temperature contours (in K) of the numerical chips with 5 μm square elements (a) Reference with 1 element of 50 μm in the width (5), (b) 1 element of 5 μm in the width (×1) and (c) 4 elements of 12.5 μm in the width (of 50 μm, ×4) after 600 μs of cutting.

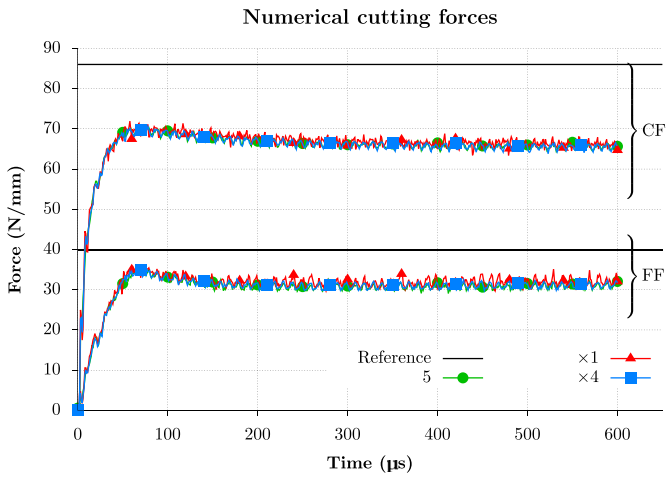

Fig. 12. Numerical cutting forces with elements width influence.

with a reasonable accuracy. To accommodate the increase of the uncut chip thickness value, the height of the workpiece is adapted. For $h = 60$ µm, $H_v = 300$ µm and for $h = 100$ µm, $H_v = 320$ µm. The corresponding numbers of nodes and elements of the models are given in Table 13.

Fig. 13 shows the four chips at $h = 60$ µm and Fig. 14 at $h = 100$ µm. In both cases, they are all continuous, as in the experimental reference, and rather similar for the same h value. With 20 µm elements, the chip is still more rounded and the gap noticed between the clearance face and the machined surface. Chips with 5 µm and 2.5 µm elements are very close to each other and no gap is observed, as expected from previous results. With 10 µm elements, the quality of the chip morphology depends on the uncut chip thickness. At 60 µm, the chip is still too much rounded and clearly less detailed than with shorter elements. At 100 µm, few significant differences are highlighted by comparison with shorter elements.

The mean values of the chip thicknesses (Tables 14 and 15) show that they are all rather close for a given uncut chip thickness. Contrary to the results at 40 µm, no clear stabilization of the mean values is observed and a slight increase occurs for smaller elements. As at 40 µm, the numerical values are larger than the experimental ones. The suggested main reason is the same: the chip cannot expand laterally in the modelling.

As previously noted, the high temperature area is in the secondary shear zone and near the tool edge radius. This area near the edge radius is smaller at 100 µm, which was expected due to the larger uncut chip thickness. This location is therefore correctly estimated. For both uncut chip thicknesses, the high temperature area is larger with 20 µm elements. Temperature fields with the three other elements sizes are very close.

Table 13
Number of elements and nodes for the models with square elements at $h = 60$ µm and $h = 100$ µm.

h (µm)	Length (µm)	Elements	Nodes
60	20	550	1196
60	10	2200	4590
60	5	8800	17,978
60	2.5	35,200	71,154
100	20	625	1352
100	10	2500	5202
100	5	10,000	20,402
100	2.5	40,000	80,802

The same observations as at 40 µm are carried out on the numerical forces evolutions (Figs. 15 and 16). Cyclic variations are obtained, although the chips are continuous. The magnitude of these variations is still larger for longer elements and their numbers are linked to that of the elements composing the mesh. Again, except with 20 µm elements, the RMS forces values are very close. The cutting forces differences with the experimental reference are less than 25% as for the uncut chip thickness of 40 µm. This confirms that the difference between experimental and numerical values are due to the choice of the JC parameters. These differences also do not increase with the uncut chip thickness, as expected, but tend to slightly decrease. The feed force modelling is usually less accurate than for the cutting force (Ducobu et al., 2016b; Karpat, 2011; Sima and Özel, 2010; Zhang et al., 2011a) and these results follow the same trend. However, the decrease of its modelling accuracy for larger uncut chip thicknesses may require to take an uncut chip thickness dependency of the friction modelling into account. The experimental values (Rech et al., 2013) on which the friction modelling is based in this study only depends on the cutting speed.

The results at the other uncut chip thicknesses values confirm that the 20 µm square elements should not be adopted for accurate modelling. The differences in the results vanish when the length of the elements decreases. A size of 5 µm is recommended as the results it leads to are nearly identical to a length of 2.5 µm and convergence is therefore reached. Longer elements will decrease the computing resources for similar results and must be privileged. Square 10 µm length elements do not lead to bad results: the chip morphology and RMS forces values are similar to converged values. The larger elements however lead to forces variations that are still significant, although they do not influence the RMS values. This elements size could therefore be adopted for fast results if rougher chip morphology is allowed (this is less significant at $h = 100$ µm) and only RMS forces values are required.

9. Conclusions

The influence of the mesh on the results of a CEL orthogonal cutting model has been studied in this paper based on the elements size, elements orientation and elements width. The following conclusions can be drawn:

- The size of the elements influences the results when it is larger than the converged value. For these large elements, artificial cyclic variations (linked to the number of elements crossed by the tool) are observed in the temporal forces evolutions, although the chip is continuous. The chip produced in these conditions has a rough shape and is too much rounded, an unrealistic gap between the clearance face and the machined surface appears as well. It is recommended to use an elements length at least two times smaller than the cutting edge radius of the tool.
- The orientation of the elements has a significant influence on the results; this was not expected to that extent. The forces evolutions are impacted but the chip morphology as well. With horizontally oriented elements, the chip is short and wide and the magnitude of the forces variations is large. Vertically oriented elements lead to long, thin and less rigid chips. The frequency of the artificial forces variations depends as well on the elements orientation. To avoid any influence of the results due to the elements orientation, it is recommended to use square elements.
- The elements width and the number of elements in the width of the model (i.e. in the direction perpendicular to the cutting plane) do not influence the results.

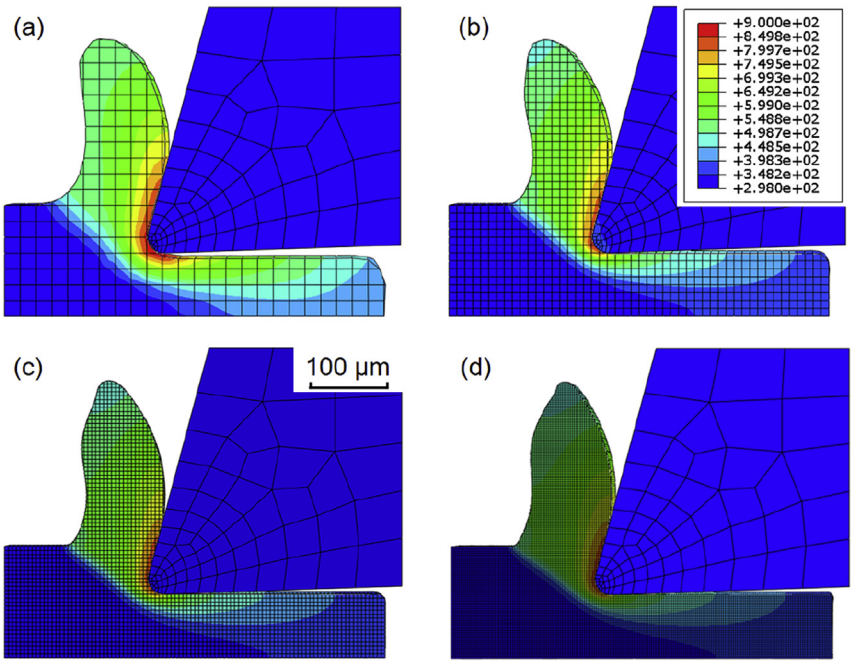

Fig. 13. Temperature contours (in K) of the numerical chips for $h = 60$ µm with square elements (a) 20 µm, (b) 10 µm, (c) 5 µm and (d) 2.5 µm after 600 µs of cutting.

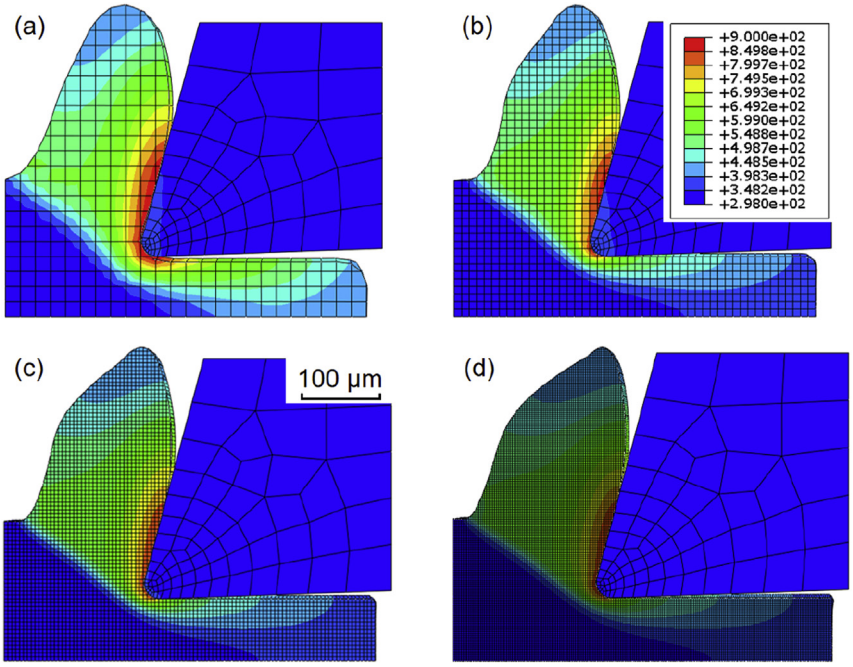

Fig. 14. Temperature contours (in K) of the numerical chips for $h = 100$ µm with square elements (a) 20 µm, (b) 10 µm, (c) 5 µm and (d) 2.5 µm after 600 µs of cutting.

Table 14
RMS cutting forces and chip thickness summary for square elements at $h = 60$ µm, Δ_x: difference with the experimental values.

Case	CF (N/mm)	Δ_{CF} (%)	FF (N/mm)	Δ_{FF} (%)	h' (µm)	$\Delta_{h'}$ (%)
Exp.	113 ± 2	–	44 ± 1	–	80 ± 4	–
20	103	9	33	25	106 ± 4	−33
10	89	21	28	36	94 ± 1	−18
5	89	21	30	32	96 ± 1	−20
2.5	88	22	31	30	99 ± 1	−24

Table 15
RMS cutting forces and chip thickness summary for square elements at $h = 100$ µm, Δ_x: difference with the experimental values.

Case	CF (N/mm)	Δ_{CF} (%)	FF (N/mm)	Δ_{FF} (%)	h' (µm)	$\Delta_{h'}$ (%)
Exp.	174 ± 2	–	50 ± 1	–	135 ± 6	–
20	149	14	30	40	159 ± 3	−18
10	135	22	26	48	153 ± 1	−13
5	133	24	28	44	157 ± 1	−16
2.5	133	24	29	42	163 ± 1	−21

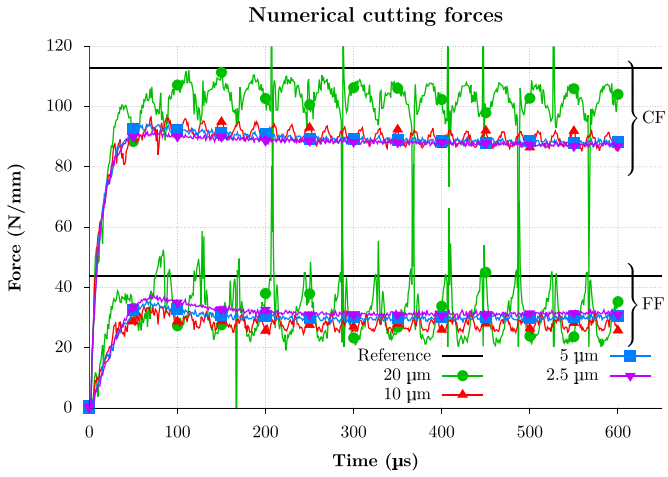

Fig. 15. Numerical cutting forces with square elements for $h = 60$ µm.

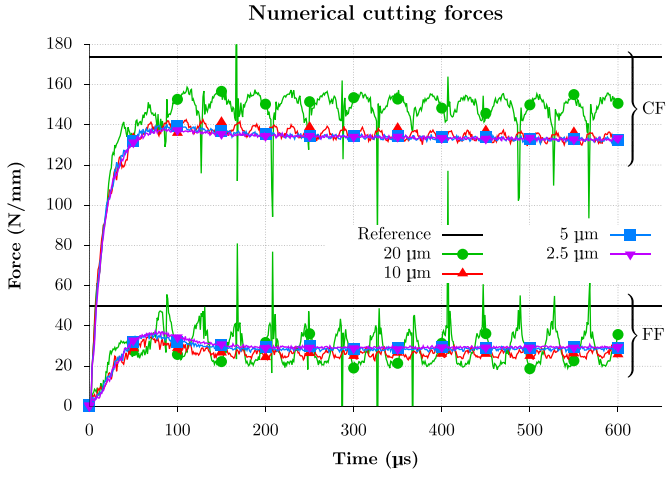

Fig. 16. Numerical cutting forces with square elements for $h = 100$ µm.

- The uncut chip thickness value influences the length of the elements at which convergence of the results is reached. A smaller uncut chip thickness requires shorter elements (10 µm elements give satisfactory results at $h = 100$ µm but 5 µm elements are required at $h = 40$ µm).
- For the cutting conditions adopted in this study, convergence is reached for 5 µm square elements. Larger elements, with a length of 10 µm, could be used to achieve fast results computing with a lower accuracy, but still satisfactory in some particular situations (only RMS forces values are required for example).

Acknowledgements

Computational resources have been provided by the supercomputing facilities of the University of Mons (Dragon1/UMONS) and the Consortium des Équipements de Calcul Intensif (CÉCI), funded by the Fonds de la Recherche Scientifique de Belgique (F.R.S.-FNRS) under Grant No. 2.5020.11. François Ducobu gratefully acknowledges Sébastien Kozlowskyj, System Manager of Dragon1, for his help and support to run Abaqus on the cluster.

References

Ambati, R., Yuan, H., 2011. FEM mesh-dependence in cutting process simulations. Int. J. Adv. Manuf. Technol. 53, 313–323.
Arrazola, P., Özel, T., Umbrello, D., Davies, M., Jawahir, I., 2013. Recent advances in modelling of metal machining processes. CIRP Ann. – Manuf. Technol. 62, 695–718.
Bäker, M., Rösler, J., Siemers, C., 2003. The influence of thermal conductivity on segmented chip formation. Comput. Mater. Sci. 26, 175–182.
Barge, M., Hamdi, H., Rech, J., Bergheau, J.M., 2006. Numerical modelling of orthogonal cutting: influence of numerical parameters. J. Mater. Process. Technol. 164–165, 1148–1153.
Bathe, K.J., Wilson, E., 1976. Numerical Methods in Finite Element Analysis. Prentice-Hall.
Cocchetti, G., Pagani, M., Perego, U., 2012. Selective mass scaling and critical time-step estimate for explicit dynamics analyses with solid-shell elements. Comput. Struct. http://dx.doi.org/10.1016/j.compstruc.2012.10.021.
Ducobu, F., Arrazola, P.J., Rivière-Lorphèvre, E., Filippi, E., 2015a. Comparison of several behaviour laws intended to produce a realistic Ti6Al4V chip by finite elements modelling. Key Eng. Mater. 651–653, 1197–1203 doi:10.4028/www.scientific.net/KEM.651-653.1197.
Ducobu, F., Rivière-Lorphèvre, E., Filippi, E., 2015b. Experimental contribution to the study of the Ti6Al4V chip formation in orthogonal cutting on a milling machine. Int. J. Mater. Form. 8, 455–468. http://dx.doi.org/10.1007/s12289-014-1189-4.
Ducobu, F., Rivière-Lorphèvre, E., Filippi, E., 2015c. On the introduction of adaptive mass scaling in a finite element model of Ti6Al4V orthogonal cutting. Simul. Model. Pract. Theory 53, 1–14. http://dx.doi.org/10.1016/j.simpat.2015.02.003.
Ducobu, F., Rivière-Lorphèvre, E., Filippi, E., 2016a. Application of the Coupled Eulerian-Lagrangian (CEL) method to the modeling of orthogonal cutting. Eur. J. Mech. - A/Solids 59, 58–66. http://dx.doi.org/10.1016/j.euromechsol.2016.03.008.
Ducobu, F., Rivière-Lorphèvre, E., Filippi, E., 2016b. Material constitutive model and chip separation criterion influence on the modeling of Ti6Al4V machining with experimental validation in strictly orthogonal cutting condition. Int. J. Mech. Sci. 107, 136–149. http://dx.doi.org/10.1016/j.ijmecsci.2016.01.008.
H.K.S., 2014. Abaqus Analysis User's Manual. Version 6.14. Dassault Systèmes.
Hortig, C., Svendsen, B., 2007. Simulation of chip formation during high-speed cutting. J. Mater. Process. Technol. 186, 66–76.
Johnson, G., Cook, W., 1983. A Constitutive Model and Data for Metals Subjected to Large Strains, High Strain Rates and High Temperatures. Proceedings of the Seventh International Symposium on Ballistics, The Hague, The Netherlands, pp. 541–547.
Karpat, Y., 2011. Temperature dependent flow softening of titanium alloy Ti6Al4V: an investigation using finite element simulation of machining. J. Mater. Process. Technol. 211, 737–749.
Koric, S., Hibbeler, L., Thomas, B., 2009. Explicit coupled thermo-mechanical finite element model of steel solidification. Int. J. Numer. Methods Eng. 78, 1–31.
Lampman, S., 1990. Wrought titanium and titanium alloys, properties and selection: nonferrous alloys and special-purpose materials. ASM Handb. ASM Int. 2, 592–633.
Meyer, H.W., Kleponis, D.S., 2001. Modeling the high strain rate behavior of titanium undergoing ballistic impact and penetration. Int. J. Impact Eng. 26, 509–521.
Nasr, M., Ng, E.G., Elbestawi, M., 2007. Effects of workpiece thermal properties on machining-induced residual stresses - thermal softening and conductivity. Proc. Inst. Mech. Eng. Part B J. Eng. Manuf. 221, 1387–1400.
Özel, T., Zeren, E., 2007. Numerical modelling of meso-scale finish machining with finite edge radius tools. Int. J. Mach. Mach. Mater. 2, 451–768.
Qiu, G., Henke, S., Grabe, J., 2011. Application of a Coupled Eulerian–Lagrangian approach on geomechanical problems involving large deformations. Comput. Geotech. 38, 30–39.
Rech, J., Arrazola, P., Claudin, C., Courbon, C., Pusavec, F., Kopac, J., 2013. Characterisation of friction and heat partition coefficients at the tool-work material interface in cutting. CIRP Ann. - Manuf. Technol. 62, 79–82.
Shams, A., Mashayekhi, M., 2012. Improvement of orthogonal cutting simulation with a nonlocal damage model. Int. J. Mech. Sci. 61, 88–96.
Sima, M., Özel, T., 2010. Modified material constitutive models for serrated chip formation simulations and experimental validation in machining of titanium alloy Ti-6Al-4V. Int. J. Mach. Tools Manuf. 50, 943–960.
Sun, J., Guo, Y.B., 2009. Material flow stress and failure in multiscale machining titanium alloy Ti-6Al-4V. Int. J. Adv. Manuf. Technol. 41, 651–659.
Umbrello, D., 2008. Finite element simulation of conventional and high speed machining of Ti6Al4V alloy. J. Mater. Process. Technol. 196, 79–87.
Zhang, Y., Mabrouki, T., Nelias, D., Gong, Y.D., 2011a. Chip formation in orthogonal cutting considering interface limiting shear stress and damage evolution based on fracture energy approach. Finite Elem. Analysis Des. 47, 850–863.
Zhang, Y., Mabrouki, T., Nelias, D., Gong, Y., 2011b. FE-model for titanium alloy (Ti-6Al-4V) cutting based on the identification of limiting shear stress at tool-chip interface. Int. J. Mater. Form. 4, 11–23.